Studies of PLD-grown ZnO and MBE-grown GaP mosaic thin films by x-ray scattering methods: beyond the restrictive ω rocking curve linewidth as a figure-of-merit.

O. Durand*[a], A. Letoublon [a], D. J. Rogers [b], F. Hosseini Teherani[b] C. Cornet [a] and A. Le Corre [a]
[a]Université Européenne de Bretagne, INSA, FOTON, UMR 6082, 20 avenue des Buttes de Coësmes, F-35708 RENNES, France
[b]Nanovation SARL, 103 bis rue de Versailles, 91400 Orsay, France
**olivier.durand@insa-rennes.fr*

ABSTRACT

X-ray scattering methods were applied to the study of thin mosaic ZnO layers deposited by Pulsed Laser Deposition on c-Al_2O_3 substrates and thin mosaic GaP layers deposited by Molecular Beam Epitaxy (MBE) on Si(001) substrates. For both systems, High Resolution (HR) studies revealed two components in the ω scans (transverse scans) which were not resolved in conventional "open-detector" ω rocking curves: a narrow, resolution-limited, peak, characteristic of long-range correlation, and a broad peak, due to defect-related diffuse-scattering giving a limited transverse structural correlation length. Thus, for such mosaic films, the conventional ω rocking curve Full Width at Half Maximum linewidth was found to be inadapted as an overall figure-of-merit for the structural quality, in that, first, the different contributions were not meaningfully represented, and, second, the linewidth depends more strongly on the film thickness than on the dispersion in the crystallographic orientation or the defect density. A "Williamson-Hall like" integral breadth (IB) metric for the HR (00.l) transverse-scans was developed as a reliable, fast, accurate and robust alternative to the rocking curve linewidth for routine non-destructive testing of such mosaic thin films. For ZnO/c-Al_2O_3 films of various thicknesses, it was deduced from the transverse scans profiles that this finite lateral correlation length may arise from misfit dislocations which accommodate the lattice-mismatch at the film-substrate interface. This WHL method is shown to be a generic approach applicable to the study of other mosaic, epitaxial, thin-film systems as illustrated through the study of mosaic GaP thin films grown by MBE on Si(001) 4°-off substrates. For this heterogeneous system, it was found from the transverse scan profiles around (002) and (006) that anti-phase crystalline domains can be evidenced. A finite correlation length associated with lateral anti-phase domain size was proposed.

I. INTRODUCTION

There is considerable technological interest in thin-film heteroepitaxy, since it opens up a wide range of new devices in the field of optoelectronics. However, it is often difficult to obtain satisfactory structural quality. This is because of the defects inherent to heteroepitaxial growth in most thin-films/substrate systems. X-ray diffraction (XRD) has proven to be a very convenient, nondestructive method for evaluating the structural quality of heteroepitaxial thin–films. "Mosaic" thin films are of particular interest.. These are layers which grow in the form of epitaxial "blocks" with rotational misorientation perpendicular to the growth direction (or "tilt") relative to one another. These monocrystalline blocks scatter X-rays incoherently with respect to each other [1][2]. The most widely adopted metric for the comparison of the crystal quality for such films is the Full-Width at Half Maximum (FWHM) (or "linewidth") of the XRD ω "rocking-curve" (performed with an open-detector). This can be misleading in the characterisation of a thin film with such a mosaic structure, however. Indeed, the rocking curve value strongly depends on the sample thickness. Therefore, in the case of epitaxial thin films, XRD ω-scan experiments ("transverse-scans"), i.e. with a channel-cut in the diffracted beam path in order to differentiate contributions orthogonal and parallel to the sample surface, should, ideally,

Oxide-based Materials and Devices II, edited by Ferechteh Hosseini Teherani, David C. Look, David J. Rogers,
Proc. of SPIE Vol. 7940, 79400L · © 2011 SPIE · CCC code: 0277-786X/11/$18 · doi: 10.1117/12.877661

be done. In this paper, we report on the development of a rapid, robust and reliable alternative to the conventional ω rocking curve figure-of-merit, which is better adapted for the characterisation of such mosaic thin films and which can be readily extracted from the XRD transverse-scans. We have applied such a method to two different "mosaic-block" optoelectronic systems, (00.1)-oriented wurtzite ZnO, deposited onto Al_2O_3 (00.1) substrates and (001)-oriented zinc-blende GaP, deposited onto 4°-off Si(001) substrates.

Wurtzite ZnO is a remarkable multifunctional material with a wide range of established and emerging applications [3][4]. These include a variety of optoelectronic uses based on a distinctive combination of properties including a direct wide bandgap (3.37eV), relatively high exciton binding energy (60meV), good transparency over the whole visible spectrum and a conductivity which can be readily tuned from semi-insulating to semi-metallic [5] to [10]. Since large area ZnO substrates are not yet available at a reasonable cost level, there is currently a need to grow ZnO on alternative substrates. The most widely adopted choice, for opto-electronic applications, is c-sapphire (c-Al_2O_3). Although, there are significant lattice and thermal mismatches [11], ZnO is a relatively compliant material [12], and it can be grown on c-Al_2O_3 in the form of epitaxial "blocks" with rotational misorientation in the film plane (or "twist") relative to one another.

Concerning the GaP/Si(001) materials system, the main interest is related to the development of Opto-Electronic Integrated Circuits (OIECs), motivated by the potential for use in optical interconnects [13]. Indeed, cost-effective, efficient, and highly integrated OEIC chips would solve issues which cannot be addressed by optics or electronics alone [14] since they will use less energy and manage much higher bandwidth with reduced electromagnetic interference than electrical communication through wires. However, one of the key components necessary for OEICs is a laser structure for efficient light emission, which cannot be Si-based due to its indirect electronic bandgap, but will more-probably be a direct-bandgap III-V compound semiconductor. The dominance of silicon (Si) in microelectronics has led to the search for OEICs based on III/V compound semiconductors integrated on Si substrates [15]. Among the different strategies for producing efficient electrically-pumped lasers on Si substrates, lattice-matched (pseudomorphic "coherent" growth) is highly preferred for the obtention of efficient and long-term stable lasers, since it does not imply the formation of threading dislocations as a result of a large lattice mismatch. In recent years, this route has been optimised through improvements in the growth of the quasi lattice-matched GaP indirect compound semiconductor on Si substrates [16]. Then, diluted-nitride GaPN-based compounds, which are known to develop a direct-band gap character, can be grown lattice-matched on GaP/Si pseudo-substrates, with an appropriate adjustment of the N content (a few percent), and can, therefore, act as efficient light emitters [17][18]. One of the major stumbling blocks in the development of efficient electrically-pumped laser devices onto Si, however, appears to be the improvement in the growth of GaP thin films on Si substrates.

In the following, we report on the development of a reliable alternative to the conventional ω rocking curve figure-of-merit, based on a Williamson-Hall-Like metric using XRD transverse-scans and applied to, (00*l*)-oriented wurtzite ZnO and zinc-blende GaP.

II. EXPERIMENTAL DETAILS

ZnO thin films were grown on c-Al_2O_3 substrates held at elevated substrate temperature in a home-made Pulsed Laser Deposition (PLD) system using a Coherent KrF excimer laser (248nm) [19]. The laser spot was focused onto a 5N sintered target to give a fluence of up to about 4 J/cm^2. During the growth, various parameters were adjusted in order to maintain a 2D growth. In particular, pulse repetition rate was varied between 1 and 50 Hz and molecular oxygen (O_2) background pressure was varied between 10^{-6} and 10^{3} Torr.

20 nm thick GaP samples were grown in a Riber Compact 21 Solid Source Molecular Beam Epitaxy (SSMBE). (001)-oriented Si substrates, intentionally offcut of 4° toward the [1 1 0], were employed, in order to favour the formation of double Si steps and minimize the appearance of Anti-Phase Domains (APD), whose presence is related to the deposition of a polar material (e.g., GaP) on a non-polar one (Si) [20]. The

growth of GaP was performed at 450°C under P_2 flux with a growth rate of 0.2 ML/s and a V/III Beam Equivalent Pressure (BEP) ratio equal to 4. Such a low temperature is expected to prevent migration of the defects from the GaP/Si interface to the volume and simultaneously favour island-like nucleation. Two growth modes were employed for comparison. The first one is the Migration Enhanced Epitaxy, called "MEE" in this paper [20]. 2ML of GaP were deposited initially to suppress the melting-back effect of Ga droplets. Then an MEE process with alternating deposition of gallium and phosphorus at the surface was adopted. This allowed a smoothing of the surface. In the second growth mode post-growth annealing was performed under phosphorus during 10 minutes at 600 °C instead of lowering the temperature to room temperature after the MEE sequence. This was assumed to improve the overall crystalline quality of the grown structure. It is called ''a-MEE'' hereafter. More details of the growth procedures can be found in reference [21].

For the ZnO samples, HRXRD and Very HRXRD (VHRXRD) experiments were conducted in Panalytical MRD-Pro and Seifert PTS systems, respectively. For both, a $Cu_{K\alpha 1}$ source (λ = 0.15406 nm) with line focus was adopted. The HR and VHR experiments were carried out using four-bounce Ge (220) and (440) crystal monochromators in the incident-beam path, giving incident-beam divergences of 12 and 5 arcsec, and wavelength dispersions ($\frac{\Delta\lambda}{\lambda}$) as low as 1.4 x 10^{-4} and 5.5 x 10^{-5}, respectively. A multilayer mirror was employed to enhance the incident intensity. Two incremental encoders allowed an angle reading to an accuracy of + 0.0002° for both the ω and 2θ positions. The HR and VHR XRD were performed, respectively, with two-bounce Ge (220) and (440) channel-cut crystals in the diffracted-beam path, giving detector acceptance angles of 12 and 5 arcsecs, respectively (i.e. 0.0033° and 0.0014°).
For the GaP samples, XRD was carried out using a Bruker AXS D8 with $Cu_{K\alpha 1}$ emission originating from a focusing monochromator. Due to the GaP films being relatively thin, no rear-back monochromator was used, in order to get sufficiently intense signal in the detector. A 0.1 mm slit was inserted after the monochromator to limit the divergence to about 0.02°. A linear multistripe detector was used to ensure a good separation of the GaP and Si signals and allow faster collection of reciprocal space maps (RSM). The transverse scans were directly extracted from RSM. In the following, 2θ is referring to the angle between the detector position and the incident beam direction and ω is referring to the angle between the incident beam direction and the sample surface. The interpretation of the results is facilitated by considering reciprocal space co-ordinates, which are related to the angular space co-ordinates by the following relationships:

$$S_x = \frac{2}{\lambda}\sin\theta\sin(\omega-\theta) \qquad (1)$$

$$S_z = \frac{2\sin\theta}{\lambda} \qquad (2)$$

where S_x and S_z are the diffraction vector along the sample surface and perpendicular to the sample surface, respectively (assuming that the diffraction planes are parallel to the sample surface, i.e. ω = θ).

III. X-RAY TRANVERSE-SCANS

In order to infer the structural quality of thin films, besides the time-consuming RSM, three HR scan modes are usually employed: ω/2θ scans which provide information on crystal planes parallel to the sample surface, rocking-curves (rotation of the sample around the ω axis, while keeping the open detector at a fixed 2θ), and ω-scans, or "transverse scans" (performed with a channel-cut crystal in the diffracted beam path)

which gives the dispersion in the orientation of the crystal planes for a given lattice spacing ("mosaïcity"), plus information on the in-plane correlation lengths. In the epitaxial thin films case, the broadening mechanisms of the diffraction peaks are due to orientation-dependent structural parameters, which lead to an anisotropic broadening of the reciprocal lattice points. Therefore, the different broadening mechanisms can be discriminated using ω/2θ and transverse scans.

For the epitaxial ZnO thin films, the growth-direction coherent-domain-size was found [22] to be comparable with the layer thickness (determined by X-Ray Reflectivity (XRR)), which indicates that there is relatively high crystalline-quality in the growth direction. Indeed, the comparatively low thickness of these ZnO layers in itself generates a widening of the ω/2θ diffraction peak, orthogonal to the sample surface, due to "crystal truncation rods", which resemble, but have nothing to do with, a defect-induced effect. Any overall measurement of the crystal quality for such films will thus include a contribution from in-plane defects. The most widely adopted metric for such measurement is the FWHM (or linewidth) of the (00.2) peak of the XRD rocking-curve. However, this metric can be misleading in the characterisation of a thin film with such a mosaic structure since the peak broadening has multiple origins including the widening due to the low-sample thickness, which is often the main source of peak widening (depending on the sample thickness). To a certain extent, the rocking-curve combines information from both the ω/2θ scans and the transverse scans. However, differentiation of the peak widening causes is desirable in order to compare samples. Therefore, in the case of such epitaxial thin films, XRD ω-scan experiments should be done with a channel-cut in the diffracted beam path ("transverse scans") in order to eliminate contributions orthogonal to the sample surface and, thereby, study only contributions parallel to the sample surface. It should be noted, also, that for such films, the Integral Breadth (IB) (defined as the width of a rectangle having the same area and height as the observed line profile) has already been put forward as a more appropriate metric than the FWHM [23].

Fig 1 shows typical transverse scans for the (00.2) reflection performed using HRXRD and which display two-component line-shapes: a very intense/narrow component (with a resolution-limited linewidth) and a broad base. In this case, the sample thickness was around 150nm. A similar response (two-component line-shape) has been observed elsewhere for a range of mosaic thin film materials [2][24] and [25] to [31] including ZnO [32][33]. The narrow and intense component is visible only in the case of weak disorder, due to an exponential damping with crystal plane displacement, and has been attributed to long-range structural correlations. This means that the plane displacements are bounded in magnitude by the substrate, which acts as a source of structural coherence (due to the epitaxy) over a relatively large lateral correlation length [2][25]. The resolution-limited character of the narrower Bragg peak linewidth in HRXRD scans was confirmed through VHRXRD (see inset of fig.1), which gave a 5" peak width. The broad diffuse-scattering peak has been attributed to diffuse-scattering for shorter-range correlation lengths and is, therefore, defect-induced [2][25]. The mosaic crystals displaying such an effect are termed "unconventional", in that individual mosaic blocks can scatter X-rays coherently with respect to each other due to long-range order, in spiteof short-range disorder.

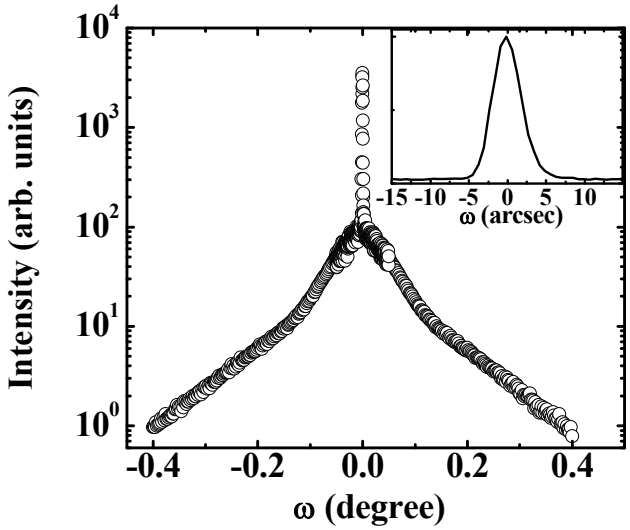

Figure 1. HR transverse scans for the (00.2) peak exhibiting a resolution-limited component and a broad base. Inset: detail of the VHR (00.2) narrow component in arcsec.

Let us notice that the two-component line-shapes, which are observed for the order (00.2) transverse scan reflection, are not resolved in the conventional "open-detector" ω rocking curve, as shown in figure 2. Although this "open-detector" ω rocking curve does not resolve the two contributions, it is clear from the peak shape that two contributions are present. Thus our prior assertion that a simple figure for the FWHM of any of these conventional "open-detector" ω rocking-curves does not adequately reflect the crystal structure of the layer is confirmed experimentally.

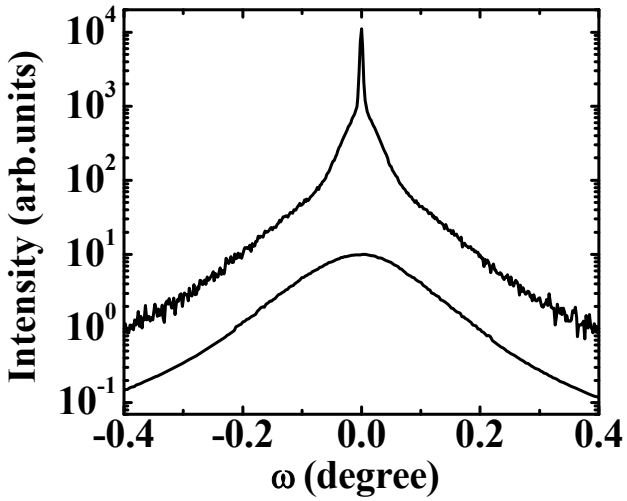

Figure 2. From top to bottom: Transverse ω scan and ω rocking-curve (open-detector)for the (00.2) peak of a 1000 nm-thick ZnO sample.

Careful inspection of the (00.2) transverse scans from two other ZnO samples, 150-nm and 70-nm thick, respectively (Fig.3) reveal satellite peaks (S), in addition to the two-component line-shapes. Such satellite peaks are rarely observed and would appear to be characteristic of a periodic lattice distortion,

originating from either a periodic arrangement of misfits or threading dislocations (which may arrange in a regular fashion in order to reduce their elastic energy [30]) or from a periodical distortion at the ZnO-c-Al_2O_3 interface (which may arise if the substrate surface is miscut, so that it forms regular terraces [24]). To differentiate between these possibilities, transverse scans were performed for different azimuthal values around the [001] axis. Since the transverse scans display the satellite peaks for azimuthal angles of both 0° (along the [1 0.0] direction) and 90° (along the [1 2.0] direction), such satellite peaks cannot arise from a miscut and are, therefore, more likely to be a characteristic of misfit or threading dislocations. It should be noted that the satellite positions vary slightly with the azimuth angle. Thus the positions of the satellites may correspond to the mean spacing between misfit or threading dislocations. For the 150 nm-thick sample this periodicity is well-defined (as revealed by the satellite sharpness) at 190 nm, for an azimuthal angle of 0°, and 235 nm, for an azimuthal angle of 90°. For the 70 nm-thick sample it was smaller (165 nm for an azimuthal angle of 0°). It is possible that the differences between the periodicities in the samples is mainly due to slight differences in the growth conditions rather than the different thicknesses. However, the relatively high value of the periodicity, and the azimuthal angles at which the peaks were observed, are not easily reconcilable with the large lattice mismatch between the ZnO and the c-Al_2O_3.

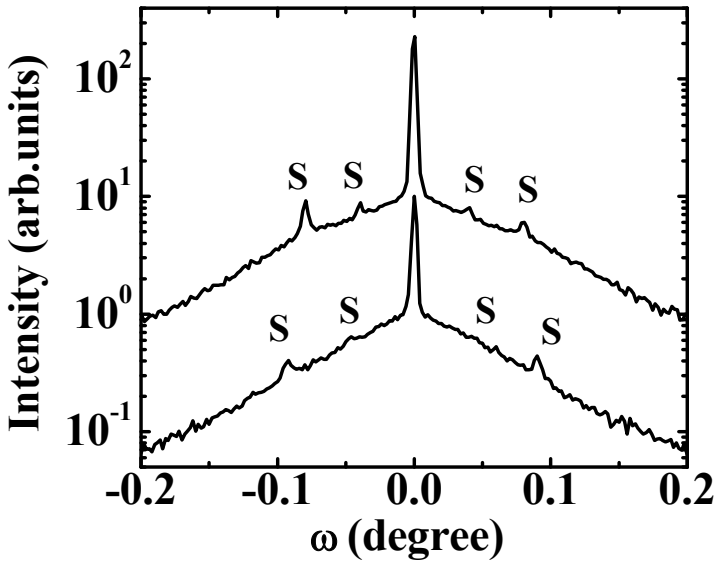

Figure 3. Transverse scans through the (00.2) diffraction peak from 2 thin ZnO layers with different thicknesses: from bottom to top: 70 nm, 150 nm, displaying satellite peaks (S).

IV MEASURE OF THE LATERAL DEFECTS CORRELATION LENGTH: WILLIAMSON-HALL-LIKE METHOD

Miceli et al [2][25] developed a phenomenological theory, which explains the broad diffuse-scattering peaks of the transverse scans as being defect-induced, and which also accounts for the presence of the narrow component in the line-profiles, in the case of ErAs/GaAs(001) thin films. In particular, they examined two extreme cases: the case of weak disorder dominated by an effect due uniquely to a lateral defect-correlation-length, ξ_x, and the case of strong disorder dominated by strains and giving a mosaic rotational disorder, $\Delta\omega$. Both cases were treated independently, using the broadening of several different diffraction order peaks

((002), (004) and (006) transverse scans), so that the peak broadening was taken as being either constant in the angular space coordinate (if its cause was purely rotational) or constant in the reciprocal space coordinate (if it was linked uniquely to a defect-correlation-length). Therefore, since the most common case is an "intermediate" case, in which the peak broadening depends on a scattering vector where both effects are combined, an appropriate "figure-of-merit" needs to incorporate both the lateral correlation length ξ_x and the mosaicity in order to compare the structural quality of different samples.

The IB method mentioned above is a fast process for deconvoluting multicomponent peaks such as those observed for mosaic thin films which is carried out using an analysis of the evolution of the peak linewidth with the scattering vector [34]. As an illustration, Fig.4 shows typical HR transverse scans obtained for different scattering vectors, i.e. the (00.2), (00.4) and (00.6) peaks, in the case of 150-nm thick ZnO films.

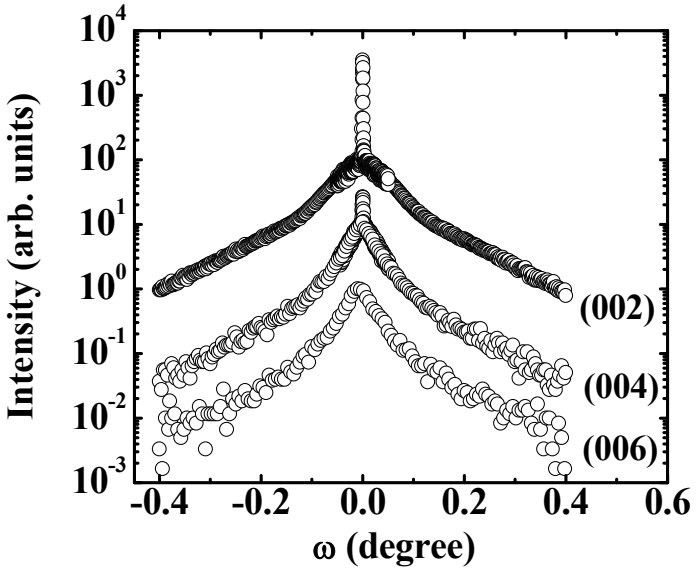

Figure 4. Typical HR transverse scans for the (00.2), (00.4) and (00.6) ZnO peaks. The HR (00.2) and the (00.4) reflections exhibit a resolution-limited component. Both the angular shape and the S-shape are different for the 3 reflections.

Both the HR (00.2) and (00.4) scans display two-component line-shapes which are not observed for the higher order (00.6) reflection. Indeed, as already reported [2][25], the peak intensity depends on the degree of disorder and decreases with increasing scattering vector modulus. Fig. 5 shows the evolution of the (00.*l*) broad-component defect-induced IB for 3 different ZnO samples (labelled samples 1, 2 and 3, respectively) versus the scattering vector. Their respective thicknesses were, from sample 1 to sample 3, 145 nm, 172 nm and 226 nm, as measured by XRR using a Fourier transform-based procedure (AutoCorrelation Function) applied to the corrected XRR profile [22][35]. Since the aim of the present paper is to develop a reliable, fast, and robust "figure-of-merit" in order to compare samples, it is beyond this scope to develop a comprehensive study of the effect of different growth parameters on the structural parameters. Only a qualitative comparison will be given as an illustration of the method.

	Peak position		Peak broadening	
Reflection hk.l	2θ (°)	S_z (nm^{-1})	β(ω) (°)	$\beta_x(S)$ (nm^{-1})
Sample 1				
(00.2)	34.3883	3.8377	0.1657	0.0111
(00.4)	72.4842	7.6751	0.1001	0.0134
(00.6)	124.9536	11.5130	0.0939	0.0189
Sample 2				
(00.2)	34.3675	3.8355	0.1918	0.0128
(00.4)	72.4757	7.6743	0.1295	0.0173
(00.6)	124.8876	11.5095	0.1335	0.0268
Sample 3				
(00.2)	34.4038	3.8394	0.1759	0.0118
(00.4)	72.5226	7.6786	0.1464	0.0196
(00.6)	125.0673	11.5189	0.1437	0.0289

Table 1. Experimentally observed peak positions and peak broadenings of the ZnO (00.*l*) reflections for samples 1, 2 and 3.

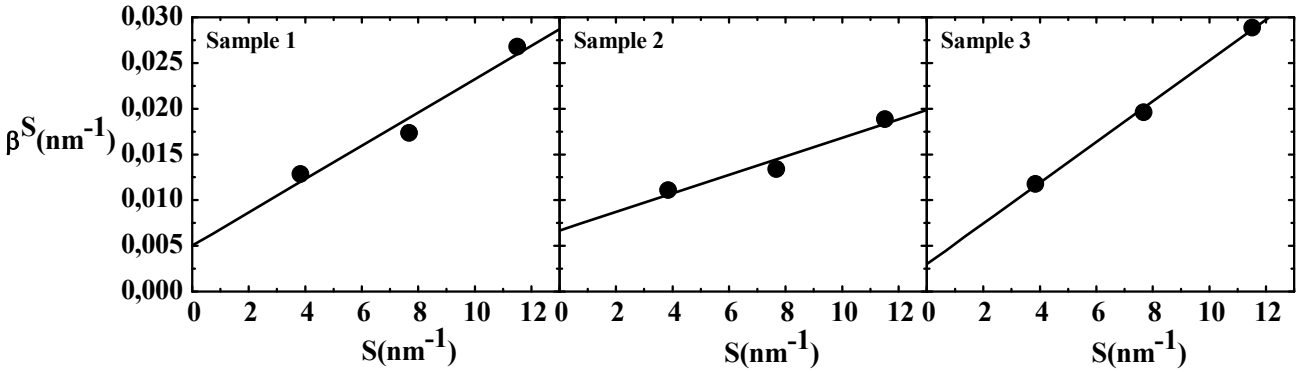

Figure 5. Evolution of the Integral Breadths for 3 ZnO samples versus the scattering vector, i.e. for the (00.2), (00.4) and (00.6) peaks

The IB method developed here uses the evolution of the (00.*l*) transverse-scans diffraction peak linewidth with the peak diffraction order (i.e. with the scattering vector modulus) in order to separate both the correlation length and mosaicity broadening, in a similar way to the Halder and Wagner parabolic approach [36][22], which is a variant of the Williamson-Hall plots method, widely used in powder diffraction to obtain a measure of both the coherent-domain-size (termed crystallite size) and the micro-strains from the linewidth analysis of the ω/2θ Bragg-Brentano diffraction peaks. The Halder and Wagner parabolic approach assumes, first, that the representation of the experimental profile is given either by a convolution of both Cauchy and Gaussian functions [37][38] (Voigt functions) or by a linear combination of these functions (pseudo-Voigt functions) [39], and, second, that the constituent profiles are either Cauchy or Gaussian. In particular, Schoening [40] plus Halder and Wagner [36] have shown that the diffraction profile from a particle (crystallite size) can be adequately modelled using a Cauchy (Lorentzian) function. They also showed that an approximation to the IB of a Voigt function is given by a parabolic equation (to an accuracy within about 5%):

$$\beta^2(s) = \beta_{Cauchy}(S).\beta(s) + \beta_{Gauss}{}^2(S) \qquad (3)$$

where β_{Cauchy} (resp. β_{Gauss}) is the IB of the Cauchy (resp. Gauss) component. In our case, $\beta(s)$ is the measured transverse-scan IB. Then, we assume that the ξ_x correlation length, extracted from the lateral reflection broadening, is similar to an average size of the crystallites [41] and, therefore can be measured using the Scherrer relation [42], as in common powder diffraction, and can be adequately modelled using a Cauchy (Lorentzian) function. In the following, $\beta_{\xi_x}(S)$ is the IB of the transverse scan diffraction peak due to broadening from the lateral correlation length ξ_x, expressed in terms of the reciprocal space coordinates. Therefore, the Scherrer relation gives $\xi_x = \frac{1}{\beta_{\xi_x}(S)}$. Second, we assume a Gaussian shape for the mosaicity-induced broadening $\beta_M(S)$ of the reflection, due to a randomly distribution of the rotational misorientation of the mosaic blocks.
This leads to the following fundamental equation:

$$(\frac{\beta(s)}{S_z})^2 = \Delta M^2 + \frac{1}{\xi_x}\frac{\beta(s)}{S_z^2} \qquad (4)$$

Where ΔM (giving the mosaicity broadening $\Delta\omega_M$) is the mosaicity tilt, due to the rotational disorder characteristic of mosaic crystals.

Therefore, the slope of $(\frac{\beta(s)}{S_z})^2$ as a function of $\frac{\beta(s)}{S_z^2}$ yields the Cauchy component due to the correlation length, ξ_x, and the intercept gives ΔM. In the following, this plot will be called the "Williamson-Hall"-like plot (WHL plot). A more detailed description of this WHL method will be published in a forthcoming paper.

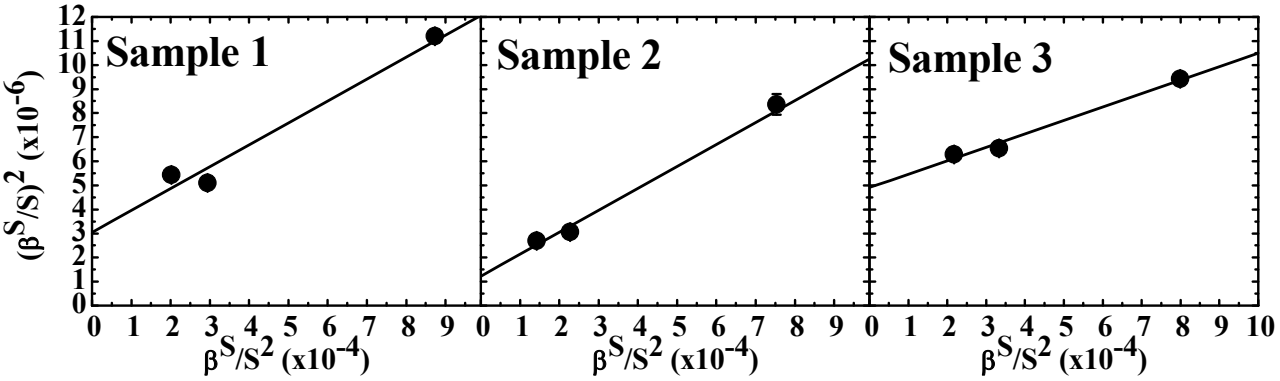

Figure 6. Analyses of the line-broadening of the diffuse scattering transverse scans, using WHL plots, for the 3 samples.

	Sample 1	Sample 2	Sample 3
Defect correlation length ξ_x	117 ± 29 nm	110 ± 9 nm	179 ± 7 nm
Mosaicity $\Delta\omega$	0.099 ± 0.002 deg.	0.063 ± 0.005 deg.	0.127 ± 0.001 deg.

Table 2. Results from the WHL plots for samples 1, 2 and 3.

Fig.6 shows the WHL plot applied to the broad components from the (00.2), (00.4) and (00.6) symmetric transverse scans, corresponding to samples 1, 2 and 3. Each transverse scan has been fitted with two Voigt functions, one for the resolution-limited narrow-component and the other for the broader component. Table 1 summarizes the input data for the WHL evaluation. Both the measured lateral correlation length ξ_x, and mosaicity $\Delta\omega$ values from the WHL analysis are summarized table 2. At a first glance, mosaicity seems to be highest when lateral correlation length is lowest. This is coherent if we consider that the lateral correlation length value is correlated to a misfit dislocation density: a lattice relaxation induced by misfit dislocations would reduce the strain-induced disorder responsible for the mosaicity. It should be noted that if the (00.2) linewidth were taken as a figure-of-merit, erroneously, and considering the lateral correlation length value (from a simple Scherrer law) the best sample would be sample 1 (90 nm), followed by sample 3 (85 nm) and sample 2 (78 nm) would be the poorest. In contrast, when considering the three (00.*l*) linewidths through the WHL analysis, sample 2 displays a lateral correlation length of 110 ± 9 nm, while sample 3 displays 179 ± 7 nm and sample 1 displays 117 nm ± 29 nm, showing that the simple linewidth measurement is not reliable even as a figure-of-merit.

V. WHL METHOD APPLIED TO ANOTHER THIN "MOSAIC-BLOCK" MATERIAL SYSTEM: CASE OF GAP/SI(001) ZINC-BLENDE THIN LAYERS

The present WHL method is generic and can be applicable to other thin "mosaic-block" material systems, e.g. (00.*l*)-oriented wurtzite materials (such as GaN, AlGaN [41], etc..) and (00*l*)-oriented zinc-blende materials (such as GaP, InAs, etc..), as illustrated in the following through the study of the quasi-lattice matched ($\Delta a/a \sim 0.4\%$) GaP/Si(001) system.

As for ZnO/sapphire, the transverse scans for the a-MEE grown GaP shown in figure 7, reveal both a sharp and a broad component for all Bragg peaks (except for the (006) for the a-MEE sample). The sharp contribution is resolution-limited, as expected. As mentioned above, one of the main issues in obtaining good structural properties in such III-V/Si systems is to minimize the appearance of APD. The scans in fig. 7 are plotted in linear intensity scale to enhance the role of both the (002) and (006) "antiphase" (weak) reflections in the study of the APD: as already stated elsewhere [43][44], the (002) and (006) reflections are sensitive to the APD (because Ga and P are in antiphase) while the (004) (strong) reflection is not sensitive to the APD. For the MEE sample, the broad contribution IB is observed to increase with increasing diffraction order whilst the ratio of sharp-to-broad contribution is observed to decrease with the *l* coordinate. For the a-MEE sample, a very different behavior is observed: firstly, the sharp-to-broad ratio in the transverse scans is much smaller than for the MEE sample. This has been interpreted as being the result of an increase in defect density with annealing. This enhancement is more obvious when looking at the (002) and (006) transverse scans, which display a more intense broad contribution compared to the (004). This is interpreted as the specific contribution of APD. These APD are coherently linked with the Si substrate, maintaining the long range lateral correlation length and contribute weakly to the (004) reflection broadening because of a weak induced lattice strain. The (002) and (006) transverse scans also exhibit very similar broad line profiles, indicating that this broadening originates from the APD [21].

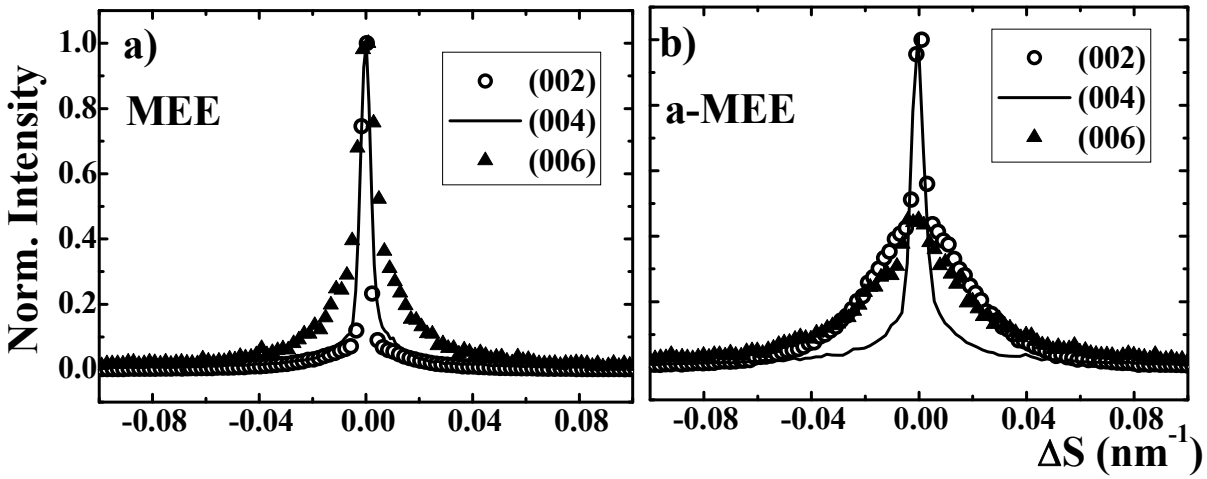

Fig. 7. 3RC ‘‘transverse’’ scans performed on GaP (002), (004) and (006) reflections for a) MEE and b) a-MEE GaP/Si samples. Intensity is normalized to the same maxima except for (006) in b) which is normalized to superimpose the (002) broad contribution.

Since (004) reflections are nearly blind to APD, they must be treated differently than (002) and (006) reflections when applying the WHL method. For the MEE sample, the evolution of both the sharp-to-broad area ratio and the IB with *l* suggest a weak contribution of the APD to broadening. Therefore, the lateral correlation length, measured through the WHL method (which gives a value of 24.7 ± 0.2 nm) is attributed to defects other than APD. The micro-mosaicity value is measured to be 0.215 ± 0.010°.

For the a-MEE sample, the WHL slope extracted from the (002) and (006) transverse scans (fig. 8b) yields an apparent lateral coherence length equal to 16.5 ± 1 nm and a micro-mosaicity below 0.01°. This lateral coherence length (ξ_{total}) is sensitive to all defects, including APD contributions. The large enhancement of the broad contribution in the 2 weak reflections, however, suggests that this correlation length corresponds mainly to the apparent APD lateral size. TEM experiments will be carried out to confirm this interpretation. The value of the lateral correlation length (ξ_{defect}) for the a-MEE sample without the APD contribution can then be inferred from the (004) integral breadth and the intercept from the previous plot (considering that the mosaicity value (ΔM) is the same for the (002), (004) and (006) diffraction planes). This gives a value of 24.4 nm, which is the same as that obtained for the MEE sample. Interpretation of this result will be given in a forthcoming paper.

	Peak position		Peak broadening	
Reflection hk.l	2θ (°)	S_z (nm^{-1})	β(ω) (°)	$\beta_x(S)$ (nm^{-1})
MEE sample				
(002)	32.732	3.658	0.727	0.0453
(004)	68.600	7.316	0.446	0.0523
(006)	115.409	10.974	0.382	0.0680
a-MEE sample				
(002)	32.732	3.658	0.967	0.0604
(004)	68.600	7.316	0.353	0.0410
(006)	115.409	10.974	0.322	0.0562

Table 3. Experimentally observed peak positions and peak broadenings of the GaP(00*l*) reflections for MEE and a-MEE samples.

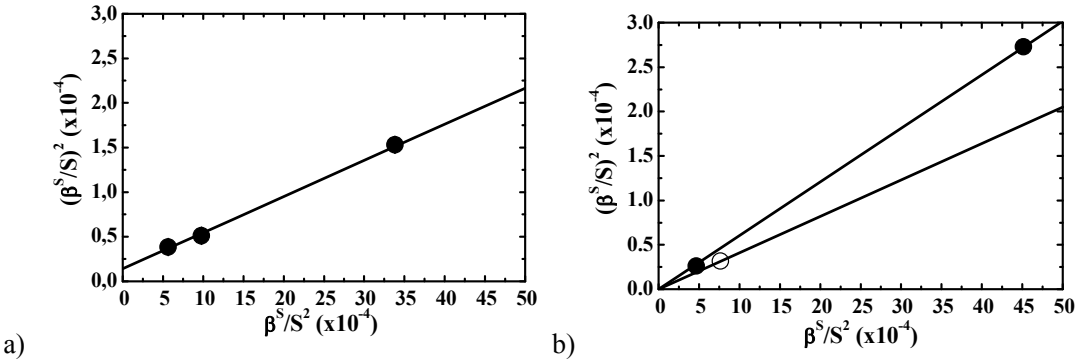

Figure 8: $(\beta(s)/S)^2$ is plotted as a function of $\beta(s)/S^2$ for three reflections for the (a) MEE and (b) a-MEE GaP/Si samples. For the a-MEE, the intercept is obtained by connecting the two weak reflection points and extrapolating to $\beta(s)/S^2=0$, then the slope corresponding to the strong reflection can be calculated.

	MEE sample	a-MEE sample
Defect correlation length $\xi_{x\ \text{weak reflections}}$	24.5 ± 1.0 nm	16.5 ± 1.0 nm
Defect correlation length $\xi_{x\ (004)}$	24.5 ± 1.0 nm	24.5 ± 2.0 nm
Mosaicity $\Delta\omega$	0.215 ± 0.010 °	< 0.01 °

Table 4. Results from the WHL plots for MEE and a-MEE GaP samples.

VI. CONCLUSION

In summary, this paper presented an analysis and interpretation of the two components which are often observed in HR X-ray scattering ω transverse scans of mosaic heteroepitaxial thin films systems. This was illustrated via studies of PLD-grown ZnO on c-Al_2O_3 substrates and MBE-grown GaP on Si substrates. A narrower, resolution-limited peak in the transverse scans, was interpreted as being characteristic of long-range structural correlation due to the epitaxy, while a broader peak was attributed to defect-related diffuse-scattering resulting from a limited transverse structural correlation length. Thus, it was suggested that the conventional "open detector" ω rocking curve linewidth was an inappropriate overall figure-of-merit for the structural quality of such mosaic films in that these different contributions were not meaningfully represented. A WHL IB metric obtained from HR (00.*l*) transverse-scans was developed as a reliable, fast, accurate and robust alternative. This method was shown to be a better approach for routine non-destructive testing of various mosaic thin film systems including (00.1)-oriented wurtzite materials (such as ZnO and GaN) and (001)-oriented zincblende materials (such as GaP and InAs).

A WHL plot method was applied as a figure-of-merit to the diffuse component in the transverse scans for three ZnO films. The measured lateral correlation length ranged from 100 nm to 180 nm and the measured $\Delta\omega$ mosaicity value ranged from 0.06 to 0.13 deg. The results are coherent with the lateral correlation length value being related to a misfit dislocation density which accommodates the lattice-mismatch at the film-substrate interface. The presence of satellite peaks in transverse ω scans was observed for films of various thicknesses. This was taken to represent a finite lateral correlation length, which may arise from misfit or threading dislocations which exhibit periodic ordering. For the GaP/Si layers, two samples were compared

with and without annealing. The marked enhancement in the intensity of the diffuse component for the (002) and (006) reflections after annealing was interpreted as the signature of APD. The WHL plot method gave an APD correlation length, for both the (002) and (006) reflections, of 16.6 ± 1 nm. The use of such an XRD method as a routine characterisation tool provides a rapid feedback for optimization of the growth process with regard to crystal quality. This method also demonstrates the importance of employing an appropriate instrumental resolution and of carrying out scans on several reflections (with different *l* indices). This latter point is critical in the context of material growth for optoelectronics and especially lasers, where crystalline perfection must be as high as possible and the problem of APD must be addressed.

REFERENCES

[1] C.G. Darwin, Philos. Mag. **43,** 800 (1922).
[2] P.F. Miceli and C.J. Palmstrom, Phys. Rev. B **51,** 5506 (1995).
[3] R. Triboulet: Proc. SPIE **4412** (2001) 1.
[4] Ü. Özgür, Ya. I. Alivov, C. Liu, A. Teke, M. A. Reshchikov, S. Dogan, V. Avrutin, S.-J. Cho, and H. Morkoç, J. Appl. Phys. **98,** 041301 (2005).
[5] K. Minegishi, Y. Kowai, Y. Kikuchi, K. Yano, M. Kasuga and A. Shimizu: Jpn. J. Appl. Phys. **36,** L1453 (1997).
[6] M. Joseph, H. Tabata and T. Kawai: Jpn. J. Appl. Phys. **38,** L1205 (1999).
[7] Y.R. Ryu, S. Zhu, D.C. Look, J.M. Wrobel, H.M. Jeong, and H.W. White, J. Crystal Growth **216**, 330 (2000).
[8] D.C. Look, D.C. Reynolds, C.W. Litton, R.L. Jones, D.B. Eason, and G. Cantwell, Appl. Phys. Lett. **81,** 1830 (2002).
[9] K-K. Kim, H -S. Kim, D-K. Hwang, J-H. Lim, and S-J. Park, Appl. Phys. Lett. **83,** 63 (2003).
[10] D.C. Look, B. Claflin, Ya. I. Alivov, and S.J. Park: Phys. Status Solidi A **201,** 2203 (2004).
[11] N. Li, E.-H. Park, Y. Huang, S. Wang, A. Valencia, B. Nemeth, J. Nause and I. Ferguson, Proc. SPIE 6337, 63370Z-1 (2006).
[12] D. J. Rogers, F. Hosseini Teherani, A. Ougazzaden, S. Gautier, L. Divay, A. Lusson, O. Durand, F. Wyczisk, G. Garry, T. Monteiro, M. R. Correira, M. Peres, A. Neves, D. McGrouther, J. N. Chapman & M. Razeghi, Appl. Phys. Lett. **91,** 071120 (2007).
[13] A. David, B. Miller, "Device Requirements for Optical Interconnects to Silicon Chips", Proceedings of the IEEE **97,** 1166 (2009).
[14] G.T. Reed, the optical age of silicon, Nature **427,** 595 (2004).
[15] D. Liang and J.E. Bowers, Nature Photonics **4,** 511 (2010)
[16] K.Volz, A. Beyer, W. Witte, J. Ohlmann, I. Németh, B. Kunert, W. Stolz, J. Crystal Growth, In Press.
[17] K.Yamane, K. Noguchi, S. Tanaka, Y. Furukawa, H. Okada, H. Yonezu, and A. Wakahara, Appl. Phys. Express **3**, 074201 (2010).
[18] B. Kunert, S.Zinnkann, K.Volz, W.Stolz, J. Cryst. Growth **310**, 4776 (2008).
[19] D. J. Rogers, F. Hosseini Téherani, A. Yasan, R. McClintock, K. Mayes, S.R.Darvish, P. Kung, M. Razeghi and G. Garry, Proc. SPIE 5732, 412 (2005).
[20] Y. Takagi, H. Yonezu, K. Samonji, T. Tsuji, N. Ohshima, J. Cryst. Growth **187,** 42 (1998).
[21] A. Létoublon, et al., J. Crys. Growth in press, doi:10.1016/j.jcrysgro.2010.10.137.
[22] O.Durand, Thin Solid Films **450,** 51 (2004).
[23] J Ian Langford and Daniel Louër, Rep. Prog. Phys. **59,** 131 (1996).
[24] Gibaud, R.A. Cowley, D.F. McMorrow, R.C.C. Ward, M.R. Wells, Phys. Rev. B **48,** 14463 (1993).
[25] P.F. Miceli, J. Weatherwax, T. Krentsel, C.J. Palmstrøm, Physica B **221,** 230 (1996).
[26] M. Becht, F. Wang, J.G. Wen, T. Morishita, J. of Crystal Growth **170,** 799 (1997).
[27] P.M. Reimer, H. Zabel, C.P. Flynn, J.A. Dura, Phys. Rev. B **45,** 11426 (1992).

[28] M. Huth, C.P. Flynn, Appl. Phys. Lett. **71,** 2468 (1997).
[29] G.L. Zhou, C.P. Flynn, Phys. Rev B **59,** 7860 (1999).
[30] V.M. Kanager, O. Brandt, H. Riechert, K.K. Saberfeld, Phys. Rev. B **80,** 033306 (2009).
[31] Boulle, R. Guinebretière, A. Dauger, J. Phys. D : Appl. Phys. **38,** 3907 (2005).
[32] Y.F. Chen, H.J. Ko, S.K. Hong, K. Inaba, Y. Segawa, T. Yao, J. of Crystal Growth **227-228,** 917 (2001).
[33] T.-B. Hur, Y.-H. Hwang, H.-K. Kim, H.-L. Park, J. Appl. Phys. **96,** 1740 (2004).
[34] H.P. Klug, L.E. Alexander, X-ray Diffraction Procedures, 2nd ed., New-York; John Wiley, 618 (1974).
[35] O.Durand, D. Rogers, F. Hosseini Teherani ,M. Andrieux, M. Modreanu, Thin Solid Films **515**, 6360 (2007).
[36] N.C. Halder, C.N.J. Wagner, Acta Crystallogr. **20,** 312 (1966).
[37] Th. H. De Keijser, J.I. Langford, E.J. Mittemeijer and A.B.P. Vogels, J. Appl. Cryst. **15,** 308 (1982).
[38] J.I. Langford, NIST Special Publication 846, Proceedings of the international conference Accuracy in Powder diffraction II, 110975 (1992).
[39] R.A. Young and D.B. Wiles, J. Appl. Cryst. **15,** 430 (1982).
[40] F.R.L. Schoening, Acta Cryst. **18,** 975 (1965)
[41] L. Kirste, K.M. Pavlov, S.T. Mudie, V.I. Punegov and N. Herres, J. Appl. Cryst. **38,** 183 (2005).
[42] P. Scherrer Nachr. Gött. **2,** 98 (1918)
[43] V.K. Dixit, T. Ganguli, T.K. Sharma, S.D. Singh, R. Kumar, S. Porwala, P. Tiwaric, A. Ingaleb, S.M. Oak., J. Cryst. Growth **310,** 3428 (2008).
[44] D.A. Neuman, H. Zabel, R. Fischer, H. Morkoc-, J. Appl. Phys. **61,** 1023 (1987).